Published in final edited form as:

Nat Biotechnol. 2020 December ; 38(12): 1431–1440. doi:10.1038/s41587-020-0572-6.

Programmable m^{6}A modification of cellular RNAs with a Cas13-directed methyltransferase

Christopher Wilson[1,2,3,†], **Peter J. Chen**[1,2,3,†], **Zhuang Miao**[1,2,3], **David R. Liu**[1,2,3,*]

[1]Merkin Institute of Transformative Technologies in Healthcare, Broad Institute of Harvard and MIT, Cambridge, MA, USA

[2]Department of Chemistry and Chemical Biology, Harvard University, Cambridge, MA, USA

[3]Howard Hughes Medical Institute, Harvard University, Cambridge, MA, USA

Abstract

N^6-methyladenosine (m^{6}A) is the most widespread internal mRNA modification in humans. Despite recent progress in understanding the biological roles of m^{6}A, the inability to install m^{6}A site-specifically in individual transcripts has hampered efforts to elucidate causal relationships between the presence of a specific m^{6}A and phenotypic outcomes. Here we demonstrate that nucleus-localized dCas13 fusions with a truncated METTL3 methyltransferase domain and cytoplasm-localized fusions with a modified METTL3:METTL14 methyltransferase complex can direct site-specific m^{6}A incorporation in distinct cellular compartments, with the former fusion protein having particularly low off-target activity. Independent cellular assays across multiple sites confirm that this targeted RNA methylation (TRM) system mediates efficient m^{6}A installation in endogenous RNA transcripts with high specificity. Finally, we show that TRM can induce m^{6}A-mediated changes to transcript abundance and alternative splicing. These findings establish TRM as a tool for targeted epitranscriptome engineering to help reveal the effect of individual m^{6}A modifications and dissect their functional roles.

Editorial summary

The most abundant RNA modification in humans, m^{6}A, can be installed at specified RNA sequences in cells, enabling functional studies.

Dynamic covalent modifications to DNA and proteins play fundamental roles in regulating gene expression[1]. RNA has recently been shown to tune gene expression through its own set

*Correspondence should be addressed to David R. Liu: drliu@fas.harvard.edu.
†These authors contributed equally

Author Contributions

C.W. and P.J.C. designed the research and performed experiments. Z.M. performed immunofluorescence experiments and assisted with plasmid cloning and RNA purification. D.R.L. designed and supervised the research. C.W., P.J.C., and D.R.L. wrote the manuscript. All authors contributed to editing the manuscript.

Competing Interests

D.R.L. is a consultant and co-founder of Beam Therapeutics, Prime Medicine, Editas Medicine, and Pairwise Plants, companies that use genome editing. D.R.L., P.J.C., and C.W. have filed patent applications on aspects of this work.

of post-transcriptional modifications, including pseudouridine (Ψ), 5-methylcytosine (m^5C), N^1-methyladenosine (m^1A), and N^6-methyladenonsine (m^6A)[2,3]. Among known endogenous cellular RNA modifications, m^6A is the most abundant within eukaryotic mRNA[4], and has been demonstrated to alter chromatin accessbility[5], RNA splicing[6], nuclear export of RNA[7], RNA stability[8,9] and translation efficiency[10] (Fig. 1a). Advances in high-throughput sequencing techniques for transcriptome-wide m^6A mapping[11,12] have also linked m^6A to a wide range of cellular functions, including stem cell proliferation and differentiation[13], cellular heat shock response[14], spermatogonia differentiation[15], maternal-to-zygotic transition[16], X-chromosome inactivation[17], DNA damage response[18], circadian clock function[19], tumorigenesis[20], long-term memory creation[21], and anti-tumor immunity[22]. Aberrant m^6A methylation has also been implicated in diseases such as acute myeloid leukemia and glioblastoma[23–25]. Despite a growing appreciation of the importance of m^6A and other RNA modifications in biology and disease, our understanding of their specific functions continues to lag far behind that of many DNA and protein modifications, in part because of the lack of methods to site-specifically install RNA modifications in a target transcript in living cells.

In humans, methylation of mRNA to form m^6A is mediated by a 184-kD heterodimer of methyltransferase-like 3 (METTL3) and methyltransferase-like 14 (METTL14)[26] (Fig. 1a). Within this complex, METTL3 catalyzes the transfer of a methyl group from *S*-adenosyl methionine (SAM) to adenine within the ssRNA sequence motif DRACH (D=A, G, or U; R=A or G; H=A, C, or U), while METTL14 scaffolds substrate RNA binding[27–29]. Along with associated accessory proteins that regulate its activity, METTL3:METTL14 co-transcriptionally methylates nascent mRNA within nuclear speckles[30]. Opposing this m^6A "writer" complex, AlkB homolog 5 (AlkBH5) and fat-mass and obesity-associated protein (FTO) oxidatively demethylate m^6A within the same DRACH motif, thus serving as "erasers"[31,32]. Within mRNA transcripts, m^6A modifications recruit "reader" proteins from the m^6A-recognizing YT521-B homology[33] (YTH) or heterogenous nuclear ribonucleoprotein (hnRNP) families[34,35] (Fig. 1a). Upon binding m^6A, these readers affect RNA splicing, nuclear export, translation, and degradation to ultimately alter the cellular abundance of methylated transcripts and their protein products[36–38]. Together, these components are thought to install, remove, and read m^6A modifications in mRNA to post-transcriptionally coordinate gene expression.

The current study of m^6A in biological processes relies on global knock down or overexpression of these m^6A writers, erasers, and readers within cells. While illuminating, such studies are limited by the bulk nature of these experiments in which the methylation state of tens of thousands of sites on many transcripts are altered, rather than focusing methylation on a single site within a transcript of interest. Tools that instead mediate programmable installation of m^6A[39] would enable the functional interrogation of specific m^6A sites and more directly reveal causal relationships between individual m^6A modifications and phenotype.

The CRISPR-associated nuclease Cas13 has been shown to bind and cleave single-stranded RNA targeted by a complementary guide RNA[40–42]. We speculated that tethering catalytically inactivated Cas13 (dCas13) to m^6A writers could allow programmable

installation of m^6A at sites specified by a Cas13 guide RNA. In this study we elucidate m^6A methyltransferase kinetics *in vitro*, fuse modified methyltransferase components to dCas13, characterize activity in bacteria and mammalian cells, and ultimately establish a targeted RNA methylation system (TRM) that enables site-directed m^6A installation in target transcripts in both the cytoplasm and nucleus (Fig. 1b). Using transcriptome-wide MeRIP-seq and differential RNA-seq, we show that off-target methylation from TRM, while detectable, is limited in scope in both bacteria and human cells. Lastly, we effect m^6A-mediated changes in RNA abundance and alternative splicing using TRM, thereby demonstrating its functional utility. By enabling programmable methylation of specific adenines within transcripts of interest with minimal perturbation of background methylation states, TRM will facilitate the elucidation of causal relationships between m^6A and biological phenotype.

Results

In vitro characterization of m^6A methyltransferase

An ideal targeted RNA methylation system maximizes the likelihood that m^6A installation occurs at the target site(s) rather than at the vast excess of non-target As in the transcriptome. To achieve high TRM specificity, we envisioned that using an m^6A methyltransferase domain with impaired substrate engagement (reflected by a modest K_m) but strong catalytic activity (k_{cat}) would make RNA methylation highly dependent on the binding of a fused dCas13 domain to the target RNA. The increase in effective molarity of RNA upon dCas13 binding in principle should selectively overcome the modest K_m for on-target RNA loci, imparting specificity.

As only METTL3 contains a SAM-dependent active site within the METTL3:METTL14 m^6A writer complex[27–29], we hypothesized that METTL3 could methylate adenine on its own and serve as a binding-impaired methyltransferase, ideal for fusion to a programmable RNA-binding protein such as dCas13. To explore this idea, we purified and measured the kinetics of METTL3 alone and the METTL3:METTL14 complex by monitoring the transfer of ^{14}C from a radiolabeled SAM cofactor to an RNA substrate[43]. Although the V_{max} of METTL3 was reduced ~3 fold in the absence of METTL14, its K_m was impaired by more than 40-fold, from 18 nM for METTL3:METTL14 to >900 nM for METTL3 (Supplementary Fig. 1). These data suggest that METTL3 or METTL3 variants may serve as ideal fusion partners to dCas13 in a TRM system, as the elevated local concentration of RNA upon dCas13 binding to the target transcript can rescue the high K_m of METTL3 alone and provide specificity for the target RNA.

Design of TRM candidate fusions

Using these insights, we selected K_m-impaired adenosine methyltransferases to fuse to dCas13. To further weaken non-specific RNA-binding affinity of full-length METTL3, we removed the zinc finger RNA-binding motifs from METTL3 to create METTL3ΔZF, referred to as M3 hereafter. While M3 could not be expressed and purified in *E. coli* in amounts sufficient for kinetic characterization, it proved to be an active and useful methyltransferase in experiments described below. In addition to M3, we also fused M3 to

the METTL3-interacting domain of METTL14 (residues 111-456, referred to as M14 hereafter) as a second binding-impaired methyltransferase candidate. Inspection of the METTL3:METTL14 heterodimer structure bound to SAM (PDB 5IL1)[28] revealed that an M14–linker–M3 fusion architecture could sterically occlude the native conformation of the heterodimer (Supplementary Fig. 2a). We therefore proceeded with M3 and M3–$(GGS)_{10}$–M14 (hereafter referred to as M3M14) as candidate methyltransferases to develop programmable RNA methylation systems.

We fused M3 and M3M14 to a catalytically inactive Cas13b variant from *Prevotella sp. P5-125* (PspCas13b Δ984-1090 H133A, referred to as dCas13 hereafter) due to its reported RNA targeting activity in RNA base editors[44,45]. Examination of the crystal structure of *Prevotella buccae* Cas13b (PbuCas13b, PDB 6DTD)[46], which shares 40% homology with PspCas13b, showed that the N-terminus is buried within the core of the protein (Supplementary Fig. 2b). We therefore tethered dCas13 by its C-terminus to M3 (dCas13–M3) and M3M14 (dCas13–M3M14) using flexible XTEN and $(SGGS)_2$-XTEN-$(SGGS)_2$ linkers[47], respectively (Fig. 2a).

Validation of TRM in bacteria

To evaluate these candidate TRM constructs in a cellular context, we first targeted RNA methylation in bacteria. We introduced into *E. coli* a DNA plasmid encoding dCas13-methyltransferase fusions under an IPTG-inducible promoter and a constitutively-expressed Cas13 guide RNA. A second plasmid encoded a synthetic target transcript containing m^6A methylation motifs (GGACU) surrounding a guide RNA-targeting sequence (Fig. 2b). To measure m^6A modification of the target transcript, we used RT-qPCR to quantify enrichment of RNA fragments immunoprecipitated with m^6A antibodies (MeRIP-RT-qPCR). We observed substantial m^6A methylation of the target substrate only upon induction of dCas13–M3 or dCas13–M3M14 expression, but not a catalytically impaired mutant methyltransferase, dCas13–$M3^{D395A}$ (dCas13–dM3) (Fig. 2c). Co-expression of active dCas13–methyltransferase fusions with a non-targeting guide RNA also resulted in minimal target methylation, establishing that guide RNA targeting is necessary for m^6A installation. We confirmed these findings with an orthogonal m^6A measurement assay in which we selectively captured the target transcript and detected m^6A by immunostaining (Supplementary Fig. 3). Collectively, these results demonstrate the ability of both dCas13–M3 and dCas13–M3M14 to methylate RNA targets in a guide RNA-programmed manner.

To assess the specificity of TRM editors in *E. coli*, we extracted and fragmented cellular mRNA after editing, then sequenced the RNA fragments enriched with m^6A antibodies (MeRIP-seq)[11,48]. For each sample, we evaluated the number of modified sites out of 42,418 RRACH m^6A motifs susceptible to off-target methylation within the *E. coli* transcriptome. We found that dCas13–M3 and the inactive dCas13–dM3 control produced 916 and 857 modified m^6A sites, respectively, of which a large majority (737) were shared in both conditions and only 179 of 42,418 possible sites were hypermethylated by dCas13–M3 (Fig. 2d). In comparison, the more active dCas13–M3M14 construct induced the methylation of 924 sites, of which 223 of 42,418 possible sites were hypermethylated compared to the inactive methylase control. These results suggest that dCas13–M3 and dCas13–M3M14 in

E. coli promote modest off-target RNA modification that correlates with their methylation activity.

Methylation of reporter transcripts in mammalian cells

Next, we sought to test site-specific m^{6}A installation in human cells. We designed guide RNAs targeting a synthetic RNA substrate placed on the 3' UTR of *Cypridina* luciferase (*Cluc*) mRNA, then targeted m^{6}A motifs surrounding the substrate's protospacer sequence with TRM editors transfected in HEK293T cells (Fig. 3a). MeRIP-RT-qPCR of this synthetic reporter (*Cluc–syn*) revealed increased (2- to 3-fold) methylation from reporter-targeted dCas13–M3 and dCas13–M3M14, but none from methyltransferase-inactive constructs (Fig. 3b). We observed a smaller increase (1.5-fold) in m^{6}A modification from dCas13–M3M14 when combined with a non-targeting guide RNA, suggesting modest off-target methylation by this construct. We confirmed these results by targeting a second reporter transcript, in which we fused the endogenous 3' UTR of the suppressor of cytokine signaling (*Socs2*) transcript onto *Cluc* (Fig. 3c). We detected similar increases in m^{6}A incorporation by dCas13–M3 and dCas13–M3M14 (1.8- to 3-fold, respectively), and once again observed modest reporter methylation (2-fold) from non-targeted dCas13–M3M14.

We performed transcriptome-wide MeRIP-seq of these TRM fusions targeting the *Cluc–Socs2* reporter to further characterize their site-specificity in human cells. In agreement with MeRIP-RT-qPCR results, MeRIP-seq revealed elevated m^{6}A enrichment at the targeted site in the presence of dCas13–M3 and dCas13–M3M14 with active methyltransferases and reporter-targeting guide RNAs (Supplementary Fig. 4a,b). We also observed a small increase in m^{6}A levels from non-targeted dCas13–M3M14, but not dCas13–M3, providing further evidence of the former's modest off-target activity. Despite these data, we only observed methylation at the intended *Socs2* 3'UTR m^{6}A sites for both editors, suggesting a high degree of TRM specificity within the targeted RNA (Supplementary Fig. 3a, b). Taken together, these results indicate that dCas13 fusions to modified methyltransferase domains can selectively and efficiently install m^{6}A on exogenous reporter RNAs in human cells, with dCas13–M3 offering especially low levels of off-target methylation.

Engineered cytoplasm- and nucleus-localized TRM editors

Since human m^{6}A readers exist within both the cytoplasm and nucleus, TRM editors localized to either part of the cell may access different RNAs and may have distinct biological properties. We therefore engineered cytoplasm- and nucleus-localized TRM construct variants by adding a nuclear export signal (NES) or nuclear localization signal (NLS) sequence to each, generating dCas13–M3nes, dCas13–M3nls, dCas13–M3M14nes, and dCas13–M3M14nls (Fig. 4a). We immunostained HEK293T cells transfected with editors bearing C-terminal HA epitopes, and confirmed that NES-tagged editors localized in the cytoplasm and both NLS-tagged editors localized in the nucleus (Fig. 4a). To investigate whether RNA targeting affects editor localization, we visualized constructs co-transfected with a guide RNA targeting the transcript of beta-actin (ACTB), which is known to mediate nuclear co-export of associated proteins[49]. Surprisingly, we observed that all editors still localized to their intended cellular compartments (Fig. 4a), suggesting minimal co-export of

nucleus-localizing constructs with *Actb* mRNA. These findings demonstrate that the intracellular localization of TRM editors can be reliably controlled with localization tags.

Next, we explored the possibility that dCas13 binding on its own may alter RNA stability or translation efficiency. We transfected HEK293T cells with nucleus- or cytoplasm-localized dCas13, a vector expressing a *Cluc* reporter transcript and *Gaussia* luciferase (*Gluc*) internal control, and guide RNAs targeting *Cluc* (Supplementary Fig. 5a). To assess RNA stability and translation of the targeted *Cluc*, we measured *Cluc* RNA abundance and luminescence activity. Using guides tiling the *Cluc* coding region, we observed that dCas13 binding did not affect *Cluc* RNA or protein levels (Supplementary Fig. 5b). As m^{6}A modifications are more commonly found within mRNA UTRs[11,48], we next targeted endogenous 5' and 3' UTRs fused to *Cluc*. We observed minimal alteration of *Cluc* RNA abundance or translation when we targeted dCas13 to the *Nanog* 3' UTR fused to *Cluc* (*Cluc–Nanog*), or the *Cluc–syn* and *Cluc–Socs2* 3' UTR reporters described above (Supplementary Fig. 5c). In contrast, targeting the 5' UTRs of *Hspa1a* and *Hsph1* fused to *Cluc* (*Hspa1a–Cluc* and *Hsph1–Cluc*, respectively) with cytoplasm-localized dCas13 resulted in up to a 61% decrease in *Cluc* protein production, but no effect on RNA abundance (Supplementary Fig. 5d). Interestingly, only cytoplasm-localized dCas13 caused this reduction, implying that 5' UTR binding may interfere with ribosome scanning and RNA translation. Taken together, these experiments suggest that dCas13 targeting does not strongly affect RNA abundance, but can reduce translation efficiency at 5' UTRs in cytoplasmic mRNA.

Methylation of endogenous transcripts in human cells

Using the above suite of cytoplasm- and nucleus-localized TRM editors, we sought to install m^{6}A modifications on endogenous transcripts in HEK293T cells. We first targeted adenine A1216 within the 3' UTR of *Actb* mRNA, which is methylated to a low degree in these cells[50]. Overexpression of METTL3 increased A1216 methylation, indicating that this site is regulated by endogenous m^{6}A writers. (Supplementary Fig. 6a). To test if TRM can direct higher levels of m^{6}A at this site in human cells, we measured *Actb* methylation resulting from all four TRM constructs with guide RNAs specific for a protospacer ending 8 bp 5' of the *Actb* A1216 site.

After transfection of these components, we observed that dCas13–M3nls and dCas13–M3M14nes robustly installed m^{6}A at *Actb* A1216, increasing methylation by 2- to 5-fold (Fig. 4b). Methyltransferase-inactive variants of these constructs, which are expressed at levels comparable to their active TRM counterparts (Supplementary Fig. 7), did not increase methylation. We also evaluated if an *Actb*-targeting guide RNA with the M3 or M3M14 methyltransferase domains alone but without dCas13 could promote dCas13-independent methylation. These components lacking dCas13 produced no increase in *Actb* methylation above that of non-targeting controls (Supplementary Fig. 6b), confirming that dCas13 is required for targeted methylation. To validate these results with an additional endogenous target transcript, we targeted A690 within the coding region of glyceraldehyde 3-phosphate dehydrogenase (GAPDH) mRNA, which is also methylated to a low extent (Supplementary Fig. 8a). Consistent with the above results, we detected substantial *Gapdh* methylation by dCas13–M3nls and dCas13–M3M14nes in a manner dependent on a *Gapdh*-targeting guide

RNA, active methyltransferase, and their fusion to dCas13 (Fig. 4c **and** Supplementary Fig. 8b,c).

To demonstrate TRM editing at biologically important m^{6}A sites, we next targeted the transcripts of forkhead box protein M1 (FOXM1), for which hypomethylation has been implicated in glioblastoma[51,52], and SRY-box 2 (SOX2), for which methylation mediates stem cell differentiation[53]. While both transcripts are endogenously methylated in HEK293T cells[12], they were amenable to further m^{6}A modification by METTL3 overexpression (Supplementary Fig. 9a **and** 10a). To determine if TRM editors could stimulate greater *Foxm1* and *Sox2* methylation, we used guide RNAs specific for their 3' UTR m^{6}A sites. In agreement with results for *Actb* and *Gapdh* targets, we found that dCas13–M3nls and dCas13–M3M14nes significantly increased m^{6}A levels of *Foxm1* (50- and 28-fold, respectively) and *Sox2* (4- and 1.7-fold, respectively) only when fused to dCas13 and supplied with targeting guide RNAs and active methyltransferase (Fig. 4d,e **and** Supplementary Fig. 9b **and** 10b).

To confirm these results with an antibody-independent, single-base resolution method, we measured site-specific m^{6}A incorporation using MazF-qPCR[54,55], which exploits the ability of m^{6}A to disrupt cleavage of ACA motifs by the ssRNA ribonuclease MazF (Supplementary Fig. 11a)[56]. Applying this method to probe two targeted adenines amenable to this approach, *Gapdh* A690 and *Sox2* A1398, we observed reduced MazF digestion of both m^{6}A sites edited by only dCas13–M3nls and dCas13–M3M14nes compared to methyltransferase-inactive editor and non-targeting guide RNA controls (Supplementary Fig. 11b,c). These results indicate increased m^{6}A modification of these targeted adenines, consistent with MeRIP-RT-qPCR results. Collectively, these results from two orthogonal methylation assays across four target transcripts establish that dCas13–M3nls and dCas13–M3M14nes can site-specifically install m^{6}A in a programmable manner.

Targeting specificity of TRM

Next, we elucidated the editing window of these two most active TRM constructs (dCas13–M3nls and dCas13–M3M14nes). We first targeted *Gapdh* A690 with a guide RNA positioned 8 bp 5' of the site, then measured methylation across the entire *Gapdh* transcript using MeRIP-seq. This experiment revealed substantially elevated m^{6}A levels at only the intended site within *Gapdh*, suggesting that TRM editors can achieve site specificity within the target mRNA (Fig. 5a,b). We similarly targeted *Actb* A1216 with TRM editors and also observed increased methylation at only this m^{6}A site within *Actb* mRNA (Supplementary Fig. 12a,b). To further characterize the TRM editing window, we tiled guide RNAs at varying distances from *Actb* A1216 and *Gapdh* A690, then measured their methylation by dCas13–M3nls and dCas13–M3M14nes. For both editors, we detected maximal *Actb* and *Gapdh* methylation using guide RNAs targeting 30 bp sites that end 8-15 bp 5' of the target adenine (Supplementary Fig. 13a,b). These results together suggest that TRM editors are most active ~10 bp 3' of the targeted protospacer on an RNA substrate and can install m^{6}A at defined adenines within a chosen transcript.

Even a small editing window of ~10 bp likely contains multiple adenines susceptible to methylation by TRM. However, we hypothesized that TRM editors might inherit the

intrinsic DRACH sequence context preference of METTL3:METTL14, which would confine TRM editing to bona fide m^{6}A motifs and confer greater specificity for a targeted m^{6}A site. To test this hypothesis, we determined the consensus sequence of m^{6}A-immunoprecipitated RNA fragments in MeRIP-seq, comparing background m^{6}A peaks to those newly installed by TRM. Neither dCas13–M3nls nor dCas13–M3M14nes substantially changed the total cellular m^{6}A consensus sequence compared to the inactive control (Supplementary Fig. 14). As the average mRNA contains only 3-5 candidate sites for m^{6}A modification[3,38], these findings suggest that TRM may be suitable to target a single adenine within a specified transcript.

Off-target methylation by TRM editors in human cells

To ensure that high TRM activity does not result in substantial non-specific methylation, we next characterized their transcriptome-wide off-target editing. We first measured the effect of TRM methylation on the total m^{6}A content within human cells by capturing cellular mRNA and staining with anti-m^{6}A antibodies. Compared to a methyltransferase-inactive control, dCas13–M3nls produced no significant difference in m^{6}A abundance (Supplementary Fig. 15). However, dCas13–M3M14nes modestly increased m^{6}A levels by 1.3-fold, suggesting a higher degree of off-target methylation for this pseudo-heterodimeric TRM construct.

To determine whether these changes in m^{6}A content affect the distribution of transcriptome-wide RNA methylation, we targeted *Gapdh* A690 with both TRM editors and profiled changes in global m^{6}A peaks using MeRIP-seq. In agreement with MeRIP-RT-qPCR data, we observed >50-fold m^{6}A enrichment of A690 by dCas13–M3nls and dCas13–M3M14nes when co-transfected with a *Gapdh*-targeting guide RNA, but not a non-targeting guide RNA (Fig. 5c,d). Examining the rest of the transcriptome revealed that dCas13–M3nls, compared to an inactive control, installed only 600-750 additional m^{6}A markers out of >21,000 detected, regardless of the guide RNA used (Fig. 5c). In contrast, dCas13–M3M14nes induced 4,000-5,500 new m^{6}A peaks (out of >21,000 detected) (Fig. 5d). To further probe this effect, we targeted *Actb* A1216 and found similar levels of non-specific methylation, with dCas13–M3M14nes generating 3- to 6-fold more off-target m^{6}A peaks than dCas13–M3nes (Supplementary Fig. 16a,b). These dCas13–M3M14nes off-targets tended to cluster on sites with low endogenous methylation, whereas dCas13–M3nls off-targets did not show this bias (Supplementary Fig. 17a,b). Consistent with this trend, dCas13–M3M14nes alters the global distribution of m^{6}A within mRNAs and lncRNAs to a larger extent than dCas13–M3nls (Supplementary Fig. 18a–e). Taken together, these data indicate that dCas13–M3M14nes methylates its non-specific substrates to a substantially greater degree than dCas13–M3nls (Fig. 5e **and** Supplementary Fig. 16c), without a clear benefit in on-target activity.

To examine whether this off-target methylation from TRM editors is sufficient to perturb a substantial fraction of the transcriptome, we performed differential RNA-seq analysis on dCas13–M3nls and dCas13–M3M14nes co-transfected with a non-targeting guide RNA. Comparison of these constructs to methyltransferase-inactive controls revealed very few (<40 out of >15,000 total genes analyzed) genes with significantly (FDR-corrected p<0.05

and >2-fold change) altered transcript abundances (Supplementary Fig. 19a,b), suggesting that off-target methylation does not by itself appreciably alter levels of cellular transcripts.

Next, we compared TRM editors to a recently described m^{6}A editor system[39] in which a METTL3-METTL14 single-chain methyltransferase domain is fused to RNA-targeting Cas9. This M3M14–dCas9 writer, unlike TRM editors, requires the delivery of a synthetic PAMmer oligonucleotide in addition to a guide RNA for targeting transcripts. To evaluate the on-target and off-target activity of M3M14–dCas9, we transfected HEK293T cells with M3M14–dCas9, PAMmer, and guide RNAs targeting *Actb* A1216, then performed MeRIP-seq. We observed >50-fold on-target m^{6}A enrichment over an inactive control, similar to results from MeRIP-seq of dCas13–M3nls and dCas13–M3M14nes (Supplementary Fig. 16a,b **and** 20a,b). However, M3M14–dCas9 supplied with non-targeting guide RNAs and PAMmers also resulted in >4-fold m^{6}A enrichment of *Actb* A1216, suggesting a substantial degree of non-specific methylation. Consistent with these findings, M3M14–dCas9 targeting *Actb* installed 2,590 additional m^{6}A modifications out of 16,800 detected (15.4%), comparable to the 3,116 off-target modifications out of 22,266 detected (14.0%) induced by dCas13–M3M14nes (Supplementary Fig. 16b **and** 20b). In contrast, dCas13–M3nls, which lacks a METTL14 RNA-binding domain, generated 5.5-fold lower frequency of off-target modifications (588 out of 21,017 detected, 2.8%) (Supplementary Fig. 16a). Thus, while all three m^{6}A writer systems exhibit comparable on-target efficiency, only dCas13–M3nls offers much reduced off-target activity.

Targeted RNA perturbation with TRM

One major effect of altering adenine methylation is to increase or decrease the expression of methylated mRNA[9,10]. For example, *Actb* A1216 methylation has been previously reported to promote *Actb* degradation[39]. To explore whether the TRM editors characterized above can result in similar changes, we targeted *Actb* A1216 with dCas13–M3nls and dCas13–M3M14nes in HEK293T cells, then performed differential RNA-seq. Compared to methyltransferase-inactive and non-targeting guide RNA controls, dCas13–M3nls and dCas13–M3M14nes caused substantial 35-42% and 45-70% decreases in *Actb* mRNA levels, respectively (Fig. 6a, b). As expected, TRM editors co-transfected with non-targeting guides did not affect *Actb* RNA amounts. These findings show that site-specific methylation is required for triggering the reduction of *Actb* mRNA levels, demonstrating that TRM editors can direct m^{6}A incorporation to influence m^{6}A-dependent RNA processing.

We next targeted the methylation of *Gapdh* A690, which has not been shown to be a physiological m^{6}A site in HEK293T cells. In contrast to the results for *Actb*, we observed that neither dCas13–M3nls nor dCas13–M3M14nes affected *Gapdh* transcript abundance (Supplementary Fig. 21a,b), despite the ability of both constructs to efficiently install m^{6}A (Fig. 4c, 5a,b, **and** Supplementary Fig. 11b). The lack of RNA abundance changes from m^{6}A incorporation in this transcript may reflect the lack of evidence that *Gapdh* A690 is interrogated by m^{6}A readers.

In addition to its effect on RNA degradation, m^{6}A has been found to mediate alternative splicing of modified pre-mRNA in the nucleus[6,34,57,58]. To determine whether nucleus-localized dCas13–M3nls could affect mRNA isoform abundances, we targeted an m^{6}A site

within the alternatively-spliced exon 21 of bromodomain-containing protein 8 (*Brd8*). We observed that methylation by dCas13–M3nls increased exon 21 exclusion by >30% (Fig. 6c), consistent with m^{6}A's known effect on *Brd8* exon skipping[57]. Treatment with non-targeting guide RNAs or methyltransferase-inactive dCas13–dM3nls abolished this effect, indicating that exon exclusion is dependent on m^{6}A installation. To investigate a second splicing target, we next methylated exon 2 of zinc finger protein 638 (*Znf638*) using dCas13–M3nls. Consistent with previous studies of m^{6}A-mediated *Znf638* splicing[58], we detected >2-fold elevated *Znf638* exon 2 inclusion driven by TRM activity (Fig. 6d). Taken together, these findings establish that TRM editors can induce two known biological consequences of m^{6}A, the degradation and alternative splicing of targeted RNA substrates, through methylation of specific adenines.

Discussion

Here we coupled the RNA targeting capability of CRISPR-Cas13 with RNA methyltransferases that generate m^{6}A to develop a targeted RNA methylation system for programmable manipulation of the epitranscriptome. We demonstrate that TRM operates broadly on a range of RNA targets with low off-targeting activity and can alter cellular processing of RNA in a methylation-dependent manner.

Beyond the clear difference in localization between the two TRM editors, dCas13–M3nls offers key advantages over dCas13–M3M14nes. First, dCas13–M3nls induces substantially less non-specific off-target methylation than dCas13–M3M14nes (Fig. 5 **and** Supplementary Fig. 16). Second, the nuclear localization of dCas13–M3nls allows targeting of mRNA 5' UTRs without a reduction in translation efficiency (Supplementary Fig. 5). Finally, m^{6}A installation by dCas13–M3nls within the nucleus preserves the opportunity for m^{6}A-modified transcripts to be recognized and regulated by nuclear m^{6}A readers, a feature we exploited to stimulate targeted changes in alternative RNA splicing (Fig. 6c,d). For these reasons, we recommend the use of dCas13–M3nls to minimize off-target activity, maximize TRM targeting scope, and allow the perturbation of m^{6}A-mediated phenotypes within the nucleus. When cytoplasmic methylation is necessary, dCas13–M3M14nes offers an alternative.

These advantages of dCas13–M3nls distinguish the TRM system developed here from the recently reported M3M14–dCas9 m^{6}A editor, which uses METTL3 and METTL14 fusions to RNA-targeting Cas9[39]. We show that the lack of a METTL14 RNA-binding domain within dCas13–M3nls results in less off-target methylation compared to dCas13–M3M14nes and M3M14–dCas9 (Fig. 5 **and** Supplementary Fig. 16 **and** 20). In addition, TRM constructs do not require any laboratory-synthesized components such as the modified PAMmer oligonucleotides[59] used by the Cas9-directed m^{6}A editor system[39], and thus can be genetically encoded in their entirety. TRM is therefore compatible with delivery strategies including viral transduction that cannot easily deliver cargo that contains a synthetic component. Finally, in contrast to M3M14–dCas9, which only functions in the cytoplasm[39], the nucleus-localized dCas13–M3nls developed in this work enables 5' UTR targeting and the ability to affect m^{6}A-dependent nuclear processing events, such as alternative splicing[58], microRNA maturation[34,60], nuclear export[7], and chromatin accessibility[5].

In light of these strengths, we anticipate that the TRM editors developed in this study will illuminate functional relationships between m^6A and phenotype, and advance basic research on m^6A biology. While additional work lies ahead to further optimize TRM efficiency and specificity, and to explore the expansion of this approach to include other RNA modifications, this study represents a key step towards the development of a precision tool kit to enable site-specific control of the epitranscriptome in cell culture and in living organisms.

Methods

General methods and molecular cloning.

TRM construct and reporter plasmids used in this study were assembled using Uracil-Specific Excision Reagent (USER) cloning. Briefly, deoxyuracil-containing primers (Integrated DNA Technologies or Eton Biosciences) were used to amplify DNA fragments with Phusion U Green Multiplex PCR Master Mix (Thermo Fisher), using polymerase chain reaction (PCR). The PCR products were electrophoresed on a 1% agarose gel containing 0.01% ethidium bromide (v/v) and imaged with a G:Box gel imager (Syngene) to confirm their identity. DNA fragments with deoxyuracil incorporated near the 5' ends were then assembled using USER Enzyme, CutSmart Buffer, and DpnI restriction enzyme (New England BioLabs) per manufacturer's protocol. To clone guide RNA plasmids, oligos encoding spacer sequences (Integrated DNA Technologies or Eton Biosciences) were annealed and golden-gate cloned into PspCas13b guide RNA cassettes. One Shot Mach1 Chemically Competent *E. coli* cells (Thermo Fisher) were transformed with assembled plasmids and grown overnight on LB agar plates with the proper maintenance antibiotic. Colonies containing correct plasmids were grown overnight in 2xYT medium with maintenance antibiotic, and plasmids were purified with either Spin Miniprep Kits (Qiagen) or Plasmid Plus Midi Kits (for mammalian cell transfections, Qiagen) with endotoxin removal. DNA concentration and purity were determined using a NanoDrop Spectrophotometer (Thermo Fisher).

Plasmid construct design.

TRM editors were constructed by fusing candidate methyltransferases to the C-terminus of PspCas13b Δ984-1090 H133A (dCas13) via an XTEN linker (SGSETPGTSESATPES) for M3 editors or an $(SGGS)_2$-XTEN-$(SGGS)_2$ linker for M3M14 editors. M3 editors used the $METTL3^{273\text{-}580}$ methyltransferase domain, and M3M14 editors used $METTL3^{359\text{-}580}$ tethered to $METTL14^{111\text{-}456}$ by a flexible $(GGS)_{10}$ linker. Nucleus-localized TRM constructs introduced an HIV nuclear localization signal (LQLPPLERLTL) at the C-terminus of dCas13, whereas cytoplasm-localized constructs incorporated SV40 bipartite nuclear export signals (KRTADGSEFESPKKKRK) at both dCas13 termini. dCas13 was amplified from pC0054-CMV-dPspCas13b-longlinker-ADAR2DD(E488Q/T375G), a gift from Feng Zhang (Addgene plasmid #103870), for subcloning into the ABE[61] plasmid backbone with constitutive expression under a CMV promoter. M3M14-dCas9 plasmids were constructed by fusing $METTL3^{369\text{-}580}$-$(GGS)_6$-$METTL14^{116\text{-}402}$ to Cas9 D10A/H840A within the pCMV-BE2 vector backbone via an XTEN linker. METTL3 and METTL14 domains in TRM editors and M3M14-dCas9 were commercially synthesized

(Genscript) with the same mammalian codon optimization. Methyltransferase-inactive TRM editors and M3M14-dCas9 constructs were generated by installing a METTL3 D395A mutation. Cas13 guide RNAs were Golden-gate cloned into pC0043-PspCas13b-crRNA, a gift from Feng Zhang (Addgene plasmid #103854), which has constitutive guide RNA expression under a U6 promoter. Cas9 guide RNAs were Golden-gate cloned into a vector bearing the *S. pyogenes* Cas9 crRNA backbone under constitutive expression by a U6 promoter.

Methyltransferase kinetics.

METTL3 and METTL3/14 complex was obtained from Active Motif (catalog #31567, 31570). The methyltransferase activity of METTL3 and METTL3-14 complex was measured using a radioactivity-based assay[43]. Radio-labeled S-adenosyl-L-methionine (^{3}H-SAM) and biotinylated unmethylated N^6-adenine single stranded RNA (ssRNA) were used as substrates (Supplementary Table 1). All assays were performed using 20 mM Tris-HCl, pH 7.5, 1 mM DTT, 0.01 %NP-40, 10U of RNaseOUT (Life Technologies) buffer. For determination of kinetic parameters, protein concentrations and reaction time were optimized to obtain linear initial velocities. To determine the K_m^{app} values for ssRNA, a saturating concentration of SAM was used (1 μM) and ssRNA substrate was titrated into the assay mixture containing the enzyme and aliquots of the reaction was stopped at various time points by heating to 90 °C for 5 min. After reaction, the biotinylated ssRNA was captured in a FlashPlate (PerkinElmer) coated with streptavidin. The amount of methylated m^{6}A ssRNA was quantified by scintillation counting (count per minute, cpm) on a TopCount microplate reader (PerkinElmer). The K_m and V_{max} values were calculated using Prism software.

Bacterial RNA purification and m^{6}A immunoprecipitation.

Chemically competent *E. coli* Tuner (DE3) cells were purchased from Millipore-Sigma. *E. coli* Tuner cells were cultured at 37 °C in LB media with shaking at 200 rpm overnight. Bacterial *E. coli* Tuner culture was pelleted by centrifuge at 6000 × g at 4 °C for 10 min. To lyse, each bacterial pellet was resuspended in preheated Max bacterial enhancement reagent (Thermo Fisher), heated at 95 °C for 5 min, and cooled on ice for 2 min. RNA was then extracted via TRIzol reagent (Thermo Fisher) and further purified with RNeasy Spin columns (Qiagen) including an on-column DNAaseI treatment to remove residual DNA. Ribosomal RNA was removed using RiboZero (Illumina). Ribo-depleted RNA was fragmented to 200-300 by addition of 50 mM $MgCl_2$ and incubated at 85 °C for 4 min.

m^{6}A immunoprecipitation (MeRIP) is based on the previously described m^{6}A-seq protocol[62] with several modifications: 30 μL of protein G magnetic beads (Thermo Fisher) were washed twice by IP buffer (150 mM NaCl, 10 mM Tris-HCl, pH 7.5, 0.1% NP-40 in nuclease-free H_2O), resuspended in 500 μL of IP buffer, and tumbled with 5 μg anti-m^{6}A antibody (New England BioLabs) at 4 °C overnight. Following 2 washes in IP buffer, the antibody-bead mixture was resuspended in 500 μL of the IP reaction mixture containing 10ug of fragmented total RNA, 100 μL of IP buffer, and 5 μL of RNasin Plus RNase Inhibitor (Promega) and incubated at least 4 h at 4 °C. After incubation the low/high salt-washing method was applied: briefly the RNA reaction mixture was washed twice in 1,000

μL of IP buffer, twice in 1,000 μL of low-salt IP buffer (50 mM NaCl, 10 mM Tris-HCl, pH 7.5, 0.1% NP-40 in nuclease-free H_2O), and twice in 1,000 μL of high-salt IP buffer (500 mM NaCl, 10 mM Tris-HCl, pH 7.5, 0.1% NP-40 in nuclease-free H_2O) for 10 min each at 4 °C. After washing, the m^6A-enriched fragmented RNA was eluted from the beads in 200 μL of RLT buffer supplied in RNeasy Mini Kit (QIAGEN) for 5 min at room temperature. The mixture was transferred to an RNA Clean & Concentrator-5 spin column (Zymo Research) and further purified via manufacturer's instructions.

Bacterial RT-qPCR.

RNA was isolated and converted to cDNA using a 1-step RNA-to-Ct (Thermo Fisher) kit according to manufacturer's protocol. RT-qPCR was performed and quantified on a CFX96 Real-Time PCR Detection System (Bio-Rad). All reactions were run in technical triplicate. Target Ct values where normalized to the geometric mean of internal controls, including an internal housekeeping gene and RNA spike-in controls to account for variability in RNA amounts. Resulting normalized values were compared to target Ct values in cells containing only the synthetic target vector using the $2^{-\Delta\Delta Ct}$ method[63].

Fluorometric targeted RNA methylation assay.

Total RNA from *E. coli* Tuner (DE3) cells was purified as described above and adjusted to a volume of 200 μL. Total RNA was denatured at 75 °C for 5 min and incubated at 42 °C for 10 min with 1 μg of dual biotin labeled DNA probe complimentary to a unique 30 base region within the synthetic target. Probe annealed target RNA was bound to 100 μL of μMACS Streptavidin microbeads (Miltenyi Biotec) and incubated at 4 °C for 15 min. Magnetic separation was done with a μColumn (Miltenyi Biotec). RNA:probe was passed over the μColumn and washed twice with 150 uL TE buffer. Probe bound RNA was eluted by adding 150 μL of H_2O warmed to 90 °C. Eluted RNA was purified and concentrated using a MiniElute column (Zymo Research). Resulting RNA concentration was determined using a Qubit RNA HS assay kit (Thermo Fisher). RNA was serial diluted and m^6A was quantified with the EpiQuik m^6A RNA methylation quantification kit (Epigentek) according to manufacturer's protocol. Flourometric m^6A signal was measured on an Infinite Pro M1000 plate reader (Tecan) at $530_{EX}/590_{EM}$ nm.

Bacterial MeRIP-seq.

Ribosomal RNA was removed using RiboZero (Illumina). Ribo-depleted RNA was fragmented to 200-300 by addition of 50 mM $MgCl_2$ and incubated at 85 °C for 4 min. RNA libraries were constructed using SMARTer PrepX Apollo NGS library prep system (Takara) following manufacturer's protocol. Libraries were normalized and ran on a NextSeq 550 sequencer (Illumina) using single-read 75 cycle kit. Resulting reads were aligned to the bacterial K12 transcriptome using HISAT2 (John Hopkins University) with reference annotation Escherichia coli strain K12 NCBI (2001). Peak calling was performed using Fisher's exact test as employed in the (m6Amonster) package considering only bins with 30 or more counts, a peak cutoff false discovery rate (FDR) of 0.05, and a peak cutoff ratio of 1. Peaks consistent between at least two replicates were kept in the final peak list.

Mammalian cell culture conditions.

All experiments involving mammalian cells were performed in HEK293T cell lines (American Type Culture Collection (ATCC)). Cells were cultured in Dulbecco's Modified Eagle Medium plus GlutaMAX (DMEM, Thermo Fisher) supplemented with 10% (v/v) fetal bovine serum (FBS). HEK293T cells were incubated at 37 °C with 5% CO_2 and maintained at confluency below 80%. Different cell passages were used for each biological replicate.

HEK293T transfection.

Unless otherwise noted, HEK293T cells were seeded on 24-well poly-D-lysine plates (Corning) at approximately 120,000 cells per well in culture medium. At 80% confluency approximately 16 h after plating, cells were transfected with 1400 ng TRM editor plasmid and 600 ng Cas13 guide RNA plasmid using 2.5 μl Lipofectamine 2000 (Thermo Fisher) in Opti-MEM I Reduced Serum Media (Thermo Fisher). A full list of Cas13 guide RNAs used in this work is given in Supplementary Table 2. For M3M14-dCas9 experiments, cells were transfected in the same manner with M3M14-dCas9 and single guide RNA plasmids at a mass ratio of 5:3. Immediately following, PAMmer oligonucleotides (Integrated DNA Technologies) were transfected using Lipofectamine RNAiMAX (Thermo Fisher) according to manufacturer's protocol. Cas9 single guide RNAs and PAMmers used in this work are shown in Supplementary Table 3. Unless otherwise noted, cells were cultured for 48 h post-transfection before total RNA extraction.

Mammalian RNA isolation and purification.

HEK293T cells were washed with PBS, then lysed with TRIzol (Thermo Fisher) and cleaned using RNeasy Mini Kit (Qiagen) or Direct-zol RNA Miniprep (Zymo Research) kits with DNaseI treatment following manufacturer's protocol. Prior to poly(A) enrichment, total RNA was supplemented with 40 nM DNA oligos (Integrated DNA Technologies, Supplementary Table 4) that hybridize to the guide RNA transfected within HEK293T cells and heated at 72 °C for 3 min. Guide-quenching oligos contained a 2',3'-dideoxycytidine modification at the 3' end to prevent primer extension in downstream reverse transcription reactions. mRNA was separated from quenched total RNA with Dynabeads $Oligo(dT)_{25}$ (Thermo Fisher) according to manufacturer's protocol.

Mammalian m^6A immunoprecipitation and RT-qPCR.

Poly(A) enriched RNA was fragmented in solution of 50 mM Tris-HCl, pH 8.0, 50 mM $MgCl_2$ and heated at 95 °C for exactly 8 min. m^6A-modified and unmodified control RNAs (New England BioLabs) were dosed into fragmented RNA, and a portion was saved as input RNA. Remaining fragmented RNA was subjected to m^6A immunoprecipitation based on the previously described m^6A-seq protocol[62] with several modifications: 30 μL of protein G magnetic beads (Thermo Fisher) were washed twice by IP reaction buffer (150 mM NaCl, 10 mM Tris-HCl, pH 7.5, 0.1% NP-40 in nuclease-free H_2O), resuspended in 500 μL of reaction buffer, and tumbled with 5 μg anti-m^6A antibody (New England BioLabs) at 4 °C overnight. Following 2 washes in reaction buffer, the antibody–bead mixture was resuspended in 500 μL of the reaction mixture containing 10 μg of fragmented total RNA,

100 μL of reaction buffer, and 5 μL of RNasin Plus RNase Inhibitor (Promega) and incubated at least 4 h at 4 °C. To remove unbound RNA, samples were washed 5 × with each of the following buffers: reaction buffer (150 mM NaCl, 10 mM Tris-HCl, pH 7.5, 0.1% NP-40 in nuclease-free H2O), low-salt reaction buffer (50 mM NaCl, 10 mM Tris-HCl, pH 7.5, 0.1% NP-40 in nuclease-free H2O), and high salt reaction buffer (500 mM NaCl, 10 mM Tris-HCl, pH 7.5, 0.1% NP-40 in nuclease-free H2O). RNA was eluted in RLT buffer (Qiagen) and purified with RNA Clean & Concentrator-5 kits (Zymo Research).

Purified RNA was reverse-transcribed with High-Capacity RNA-to-cDNA (Thermo Fisher) according to manufacturer's protocol. Resulting cDNA was pre-amplified with SsoAdvanced PreAmp Supermix (Bio-Rad) using qPCR forward and reverse primers (Supplementary Table 5) according to manufacturer's protocol. qPCR was performed with IQ Multiplex Powermix (Bio-Rad) using TaqMan probes (Bio-Rad) specific for the targeted m^6A site and reference controls (Supplementary Table 5). All reactions were performed and quantified on a CFX96 Real-Time PCR Detection System (Bio-Rad) in technical triplicate. For m^6A target sites with multiple probes, the geometric mean was taken for the resulting Ct qPCR values. To account for variability in RNA amounts, target Ct values where normalized to the geometric mean of the following internal controls: a methylated EEF1A1 control transcript, m^6A-modified RNA spike-in controls (New England BioLabs), and a non-targeted region on the TRM-targeted transcript. Resulting normalized values were compared to target Ct values from a pUC19-only transfection control using the $2^{-\Delta\Delta Ct}$ method[63].

Immunofluorescence microscopy.

A 3× hemagglutinin (3×HA) epitope tag (YPYDVPDYAYPYDVPDYAYPYDVPDYA) was cloned onto the C-terminus of TRM editor constructs. HEK293T cells were grown on poly-D-lysine/laminin 12 mm coverslips (Corning) placed on 24-well plates. At 60% confluency, each coverslip was transfected with 125 ng 3×HA-tagged editor plasmid and 375 ng guide RNA plasmid, using 1 μL Lipofectamine 2000 (Thermo) according to manufacturer's protocol. After 48 h of incubation, culture media was aspirated, and coverslips were washed once with PBS. Cells were fixed by incubating in 4% PFA (Electron Microscopy Sciences) for 30 min. Cells were then washed with PBS 3 × and permeabilized with PBS + 0.1% Triton (PBST) for 1 h at room temperature. Cells were stained with a mouse anti-HA primary antibody (1:100, Cell Signaling Technology 2367) in blocking buffer (3% BSA in PBST) for 12 h at 4 °C. Cells were then washed 5 × with PBST and stained with a goat anti-mouse IgG, AF488 secondary antibody (1:800, Thermo Fisher A-11029) in blocking buffer for 1 h at room temperature. Cover slips were finally washed 3 × with PBST and mounted onto microscope slides (VWR) with ProLong Diamond Antifade Mountant with DAPI (Invitrogen). Images were acquired using an Axioplan 2 fluorescence microscope (Carl Zeiss) and analyzed with MetaMorph version 7.8 and ImageJ version 2.0.0-rc-69/1.52i.

Measurement of luciferase RNA and protein expression.

To generate luciferase reporter constructs, *Cypridina* luciferase (Cluc) driven by a CMV promoter and *Gaussia* luciferase (Gluc) driven by an EF1-α promoter were cloned onto the same vector. 5' UTR and 3' UTR sequences for Cluc reporters were synthesized (Integrated

DNA Technologies) and cloned onto Cluc. Both luciferases were expressed from the same vector, allowing Gluc to serve as a dosing control for Cluc targeting.

For luciferase experiments, HEK293T cells were plated at 20,000 cells per well in 96-well culture plates (VWR). Each well was transfected at 75% confluency 16 h later with 250 ng TRM editor plasmid, 150 ng Cas13 guide RNA plasmid, and 12.5 ng dual-luciferase reporter vector using 0.5 μL Lipofectamine 2000 (Thermo Fisher) according to the manufacturer's protocol. Cells were cultured for 48 h post-transfection before media containing secreted luciferase was removed. Luciferase activity was measured from 20 μl of harvested media diluted 1:5 in PBS using Pierce *Cypridina* and Pierce *Gaussia* Luciferase Flash Assay kits (Thermo Fisher). All luciferase activity measurements were performed as biological replicates on a Biotek Synergy 4 plate reader with an injection protocol.

To measure luciferase transcript abundance, RNA was isolated and converted to cDNA using a 2-step Cells-to-Ct (Thermo Fisher) kit with 10 min (2× longer than suggested) DNaseI treatment to ensure degradation of plasmid DNA. All other steps were carried out according to manufacturer's protocol. qPCR was performed on a CFX96 Real-Time PCR Detection System (Bio-Rad) with technical and biological triplicates using TaqMan probes (Bio-Rad) for Cluc and Gluc transcripts. Samples for luciferase activity measurement and luciferase RNA quantification were taken from the same cells. For both RNA and protein measurement, Cluc signal was normalized by Gluc dosing control.

Western blotting.

HEK293T cells in 6-well plates were transfected with 2.8 μg 3×HA-tagged TRM editor and 1.2 μg non-targeting guide RNA. After 48 h, cells were washed with PBS and lysed in 200 μl RIPA buffer (Thermo Fisher) with PMSF and cOmplete Protease Inhibitor Cocktail (Roche). Lysate was denatured at 95 °C, 1 μl per sample was loaded into a 10-well NuPAGE 4-12% Bis-Tris gel (Thermo Fisher), and gel was dry-transferred to a 0.2 μm PVDF (polyvinylidene difluoride) membrane (Thermo Fisher) using an iBlot 2 Dry Blotting System (Thermo Fisher) for 7 min at 20 V. Membranes were stained with mouse anti-HA (1:1000, Cell Signaling Technology 2367) and rabbit anti-Histone H3 (1:2500, Abcam ab1791) in Odyssey Blocking Buffer in TBS (LI-COR) overnight at 4 °C. After washing 3× with TBST (TBS + 0.5% Tween-20), membranes were incubated with IRDye-labeled secondary antibodies goat anti-mouse 680RD (LI-COR 926-68070) and donkey anti-rabbit 800CW (LI-COR 926-32213) diluted 1:5000 in Odyssey Blocking Buffer for 1 h at room temperature. The membrane was finally washed 3× with TBST, then imaged on an Odyssey Imaging System (LI-COR).

MazF single nucleotide m^{6}A modification detection.

10 technical replicates of 3 biological replicates of polyA+ RNA were plated in a 384 well PCR plate (Applied Biosystems) using a Mantis microfluidic dispensing system (FORMULATRIX), facilitating precise dispensing at small volumes. RNA was prepared by mixing 15 ng of polyA-enriched RNA in two conditions: One containing 10 units of MazF enzyme (Takara), MazF buffer (40mM Na2P04 pH 7.5, 0.05% Tween 20), and 1 U of RNaseOUT; and the other containing MazF buffer and RNaseOUT only. Cleavage and

control reactions were incubated at 37 °C for 30 min and then heat denatured for 4 min to stop the cleavage reaction. MazF treated and control samples where reverse transcribed using the High-Capacity RNA-to-cDNA (Thermo Fisher) kit according to the manufacturer's protocol at 1/4 volume added using Mantis microfluidic dispensing system. Differential MazF cleavage of the target RNA transcript was quantified by qPCR with IQ Multiplex Powermix (Bio-Rad) using two TaqMan probes (Bio-Rad) one targeting the cleavage site the other targeting an uncleaved section of the target transcript. All reactions were performed and quantified on a CFX384 Real-Time PCR Detection System (Bio-Rad).

MeRIP-sequencing.

Total RNA from 4 biological replicates of each condition was poly(A)-enriched using Dynabeads Oligo$(dT)_{25}$ (Thermo Fisher) and fragmented to a mean size of 200-300 nucleotides by incubation in 50 mM $MgCl_2$ for 8 min at 95 °C. A portion of fragmented RNA was saved as input. Remaining RNA samples were incubated overnight at 4 °C rotating with protein G magnetic beads (Thermo Fisher) coated with EpiMark anti-m^6A antibody (New England BioLabs). Washes and elution were performed on a Biomek liquid handler (Beckman Coulter). To remove unbound RNA, samples were washed five times with each of the following buffers: reaction buffer (150 mM NaCl, 10 mM Tris-HCl, pH 7.5, 0.1% NP-40 in nuclease-free H2O), low-salt reaction buffer (50 mM NaCl, 10 mM Tris-HCl, pH 7.5, 0.1% NP-40 in nuclease-free H2O), and high salt reaction buffer (500 mM NaCl, 10 mM Tris-HCl, pH 7.5, 0.1% NP-40 in nuclease-free H2O). RNA was eluted with RLT buffer (Qiagen) and purified with MyOne Silane Dynabeads (Thermo Fisher). RNA libraries for the RNA input, collected supernatant, and IP were constructed using SMARTer PrepX Apollo NGS library prep system (Takara) following the manufacturer's protocol. The size distributions of the resulting libraries were assessed using the Tapestation D1000 screen tape (Agilent Technologies), normalized, and sequenced on a NextSeq 550 (Illumina) using a single read 75 cycle kit.

MeRIP sequencing analysis.

MeRIP-seq reads were trimmed for quality using the TrimGalore version 0.6.2 aligned to the human transcriptome using HISAT2 (Johns Hopkins University) with reference annotation UCSC hg38. For transcriptome-based methylation detection, the R package MeTDiff was used to detect differential m^6A methylation[64]. m6A peak calling and differential methylation of the transcriptome was evaluated using five input and IP replicates for each condition with peak cutoff and peak differential cutoffs set to 0.05 and reads with a mapping quality < 20 filtered out. MeTDiff calculates *P* values using a logs likelihood-ratio test with Benjamini-Hochberg false discovery rate correction. We created a consensus list of peaks by including peaks that were consistent between three samples. Peaks consistent between at least 3 replicates where kept in the final consensus peak list. The top 4,000 peaks where selected for *de novo* motif discovery and performed using HOMERv4.10.[65] The Guitar R package was used to plot mRNA and lnRNA density coverage.

Quantification of mRNA m^6A content.

mRNA was purified from HEK293T cells co-transfected with TRM editors and non-targeting guide RNAs. RNA concentration was quantified with Qubit RNA HS Assay

(Thermo Fisher) and normalized to 18.75 ng/μL. To measure % m^6A, 150 ng (8 μL) of diluted mRNA was used for the EpiQuik m^6A RNA methylation quantification kit (Epigentek) according to manufacturer's protocol. A standard curve and both negative and positive controls were used. Colorimetric m^6A signal was measured at 450 nm on an Infinite Pro M1000 plate reader (Tecan) and sample absorbance was subtracted from negative control background absorbance for analysis.

RNA-sequencing.

HEK293T cells were transfected with TRM editors combined with non-targeting guide RNAs and total RNA was harvested after 48 h. Total RNA was polyA enriched as described above. Sequencing libraries were prepared using polyA-enriched RNA on a SMARTer PrepX Apollo NGS library prep system (Takara) following manufacturer's protocols. Libraries were normalized with a Qubit dsDNA HS Assay (Thermo Fisher) and sequenced on a NextSeq 550 (Illumina) using high output v2 kits (Illumina) with 75 cycles. Reads were aligned to a custom hg38 transcriptome containing dCas13 with reference UCSC hg38. Fastq files were filtered with TrimGalore version 0.6.2 (https://github.com/FelixKrueger/TrimGalore) to remove low-quality bases, unpaired sequences, and adaptor sequences. Trimmed reads were aligned to a *Homo sapiens* genome assembly GRCh38 with a custom Cas13 gene entry by aligning reads with STAR version 2.7.0d (1st pass) followed by a second STAR alignment using generated splice sites from the 1st pass to create a 2-pass STAR Alignment. RSEM version 1.3.1 was used to quantify transcript abundance. The limma-voom package[66,67] was used to normalize gene expression levels and perform differential expression analysis with batch effect correction.

Measurement of alternative splicing.

HEK293T cells were plated at 20,000 cells per well in 96-well culture plates (VWR). Each well was transfected at 75% confluency with 250 ng TRM editor plasmid and 150 ng Cas13 guide RNA plasmid using 0.5 μL Lipofectamine 2000 (Thermo Fisher) according to the manufacturer's protocol. As a vector control, 400 ng of pUC19 plasmid was also transfected. After 48 h post-transfection, RNA was isolated and converted to cDNA using a 2-step Cells-to-Ct (Thermo Fisher) kit with 10 min (2× longer than suggested) DNaseI treatment to ensure degradation of genomic DNA. All other steps were carried out according to manufacturer's protocol. Semi-quantitative PCR was performed in 20 μL reactions with Q5 Hot-Start High-Fidelity DNA Polymerase (New England BioLabs), 1 μL of cDNA, and 0.5 μM of each forward and reverse primer (Integrated DNA Technologies, Supplementary Table 6). All PCR reactions were performed for 35 cycles. Amplified cDNA was diluted 1:20 in nuclease-free H_2O then run on a Tapestation D1000 or D5000 screen tape (Agilent Technologies). Size abundances of each splicing isoform were integrated to quantify exon exclusion and inclusion.

Life Sciences Reporting Summary.

Further information on experimental design is available in the Nature Research Reporting Summary linked to this article.

Data Availability.

Key plasmids from this work are available from Addgene (depositor: David R. Liu) and other plasmids are available upon request. All unmodified reads for sequencing-based data in the manuscript are available on the NCBI Sequence Read Archive, accession number PRJNA559201. Amino acid sequences of TRM editors reported in this study are provided in the Supplementary Sequences.

Code Availability.

All scripts used in this study are available at https://github.com/CwilsonBroad/

Supplementary Material

Refer to Web version on PubMed Central for supplementary material.

Acknowledgements

We thank the Harvard Bauer Core facility staff for assistance with automatic liquid handling and NGS library preparation; J. Nelson, A. Anzalone, and R. Chen for helpful discussions; the Pattern team at the Broad Institute for data visualization assistance; and A. Hamidi for assistance editing the manuscript. This work was supported by the Ono Pharma Foundation, U.S. NIH RM1 HG009490, U01 AI142756, and R35 GM118062, and HHMI. C.W. is the Marion Abbe Fellow of the Damon Runyon Cancer Research Foundation (DRG-2343-18). P.J.C. is supported by an NSF Graduate Research Fellowship.

References

1. Goldberg AD, Allis CD & Bernstein E Epigenetics: a landscape takes shape. Cell 128, 635–638, doi:10.1016/j.cell.2007.02.006 (2007). [PubMed: 17320500]
2. Hoernes TP & Erlacher MD Translating the epitranscriptome. Wiley Interdiscip Rev RNA 8, doi:10.1002/wrna.1375 (2017).
3. Zhao BS, Roundtree IA & He C Post-transcriptional gene regulation by mRNA modifications. Nat Rev Mol Cell Biol 18, 31–42, doi:10.1038/nrm.2016.132 (2017). [PubMed: 27808276]
4. Meyer KD & Jaffrey SR The dynamic epitranscriptome: N6-methyladenosine and gene expression control. Nature reviews. Molecular cell biology 15, 313–326, doi:10.1038/nrm3785 (2014). [PubMed: 24713629]
5. Liu J et al. N(6)-methyladenosine of chromosome-associated regulatory RNA regulates chromatin state and transcription. Science, eaay6018, doi:10.1126/science.aay6018 (2020).
6. Xiao W et al. Nuclear m(6)A Reader YTHDC1 Regulates mRNA Splicing. Molecular cell 61, 507–519, doi:10.1016/j.molcel.2016.01.012 (2016). [PubMed: 26876937]
7. Roundtree IA et al. YTHDC1 mediates nuclear export of N(6)-methyladenosine methylated mRNAs. Elife 6, doi:10.7554/eLife.31311 (2017).
8. Shi H et al. YTHDF3 facilitates translation and decay of N(6)-methyladenosine-modified RNA. Cell Res 27, 315–328, doi:10.1038/cr.2017.15 (2017). [PubMed: 28106072]
9. Wang X et al. N6-methyladenosine-dependent regulation of messenger RNA stability. Nature 505, 117–120, doi:10.1038/nature12730 (2014). [PubMed: 24284625]
10. Wang X et al. N(6)-methyladenosine Modulates Messenger RNA Translation Efficiency. Cell 161, 1388–1399, doi:10.1016/j.cell.2015.05.014 (2015). [PubMed: 26046440]
11. Dominissini D et al. Topology of the human and mouse m6A RNA methylomes revealed by m6A-seq. Nature 485, 201–206, doi:10.1038/nature11112 (2012). [PubMed: 22575960]
12. Meyer Kate D. et al. Comprehensive Analysis of mRNA Methylation Reveals Enrichment in 3′ UTRs and near Stop Codons. Cell 149, 1635–1646, doi:10.1016/j.cell.2012.05.003 (2012). [PubMed: 22608085]

13. Batista PJ et al. m(6)A RNA modification controls cell fate transition in mammalian embryonic stem cells. Cell stem cell 15, 707–719, doi:10.1016/j.stem.2014.09.019 (2014). [PubMed: 25456834]
14. Zhou J et al. Dynamic m(6)A mRNA methylation directs translational control of heat shock response. Nature 526, 591–594, doi:10.1038/nature15377 (2015). [PubMed: 26458103]
15. Xu K et al. Mettl3-mediated m(6)A regulates spermatogonial differentiation and meiosis initiation. Cell Res 27, 1100–1114, doi:10.1038/cr.2017.100 (2017). [PubMed: 28809392]
16. Zhao BS et al. m(6)A-dependent maternal mRNA clearance facilitates zebrafish maternal-to-zygotic transition. Nature 542, 475–478, doi:10.1038/nature21355 (2017). [PubMed: 28192787]
17. Patil DP et al. m(6)A RNA methylation promotes XIST-mediated transcriptional repression. Nature 537, 369–373, doi:10.1038/nature19342 (2016). [PubMed: 27602518]
18. Xiang Y et al. RNA m6A methylation regulates the ultraviolet-induced DNA damage response. Nature 543, 573–576, doi:10.1038/nature21671 (2017). [PubMed: 28297716]
19. Zhong X et al. Circadian Clock Regulation of Hepatic Lipid Metabolism by Modulation of m(6)A mRNA Methylation. Cell reports 25, 1816–1828 e1814, doi:10.1016/j.celrep.2018.10.068 (2018). [PubMed: 30428350]
20. Jaffrey SR & Kharas MG Emerging links between m(6)A and misregulated mRNA methylation in cancer. Genome medicine 9, 2, doi:10.1186/s13073-016-0395-8 (2017). [PubMed: 28081722]
21. Zhang Z et al. METTL3-mediated N(6)-methyladenosine mRNA modification enhances long-term memory consolidation. Cell Res 28, 1050–1061, doi:10.1038/s41422-018-0092-9 (2018). [PubMed: 30297870]
22. Han D et al. Anti-tumour immunity controlled through mRNA m(6)A methylation and YTHDF1 in dendritic cells. Nature 566, 270–274, doi:10.1038/s41586-019-0916-x (2019). [PubMed: 30728504]
23. Engel M & Chen A The emerging role of mRNA methylation in normal and pathological behavior. Genes Brain Behav, doi:10.1111/gbb.12428 (2017).
24. Jaffrey SR & Kharas MG Emerging links between m6A and misregulated mRNA methylation in cancer. Genome medicine 9, 2, doi:10.1186/s13073-016-0395-8 (2017). [PubMed: 28081722]
25. Cui Q et al. m6A RNA Methylation Regulates the Self-Renewal and Tumorigenesis of Glioblastoma Stem Cells. Cell reports 18, 2622–2634, doi:10.1016/j.celrep.2017.02.059 (2017). [PubMed: 28297667]
26. Liu J et al. A METTL3-METTL14 complex mediates mammalian nuclear RNA N6-adenosine methylation. Nat Chem Biol 10, 93–95, doi:10.1038/nchembio.1432 (2014). [PubMed: 24316715]
27. Sledz P & Jinek M Structural insights into the molecular mechanism of the m(6)A writer complex. Elife 5, doi:10.7554/eLife.18434 (2016).
28. Wang X et al. Structural basis of N(6)-adenosine methylation by the METTL3-METTL14 complex. Nature 534, 575–578, doi:10.1038/nature18298 (2016). [PubMed: 27281194]
29. Wang P, Doxtader KA & Nam Y Structural Basis for Cooperative Function of Mettl3 and Mettl14 Methyltransferases. Mol Cell 63, 306–317, doi:10.1016/j.molcel.2016.05.041 (2016). [PubMed: 27373337]
30. Scholler E et al. Interactions, localization, and phosphorylation of the m(6)A generating METTL3-METTL14-WTAP complex. RNA 24, 499–512, doi:10.1261/rna.064063.117 (2018). [PubMed: 29348140]
31. Zheng G et al. ALKBH5 is a mammalian RNA demethylase that impacts RNA metabolism and mouse fertility. Mol Cell 49, 18–29, doi:10.1016/j.molcel.2012.10.015 (2013). [PubMed: 23177736]
32. Jia G et al. N6-methyladenosine in nuclear RNA is a major substrate of the obesity-associated FTO. Nat Chem Biol 7, 885–887, doi:10.1038/nchembio.687 (2011). [PubMed: 22002720]
33. Wang X & He C Reading RNA methylation codes through methyl-specific binding proteins. RNA Biol 11, 669–672, doi:10.4161/rna.28829 (2014). [PubMed: 24823649]
34. Alarcon CR et al. HNRNPA2B1 Is a Mediator of m(6)A-Dependent Nuclear RNA Processing Events. Cell 162, 1299–1308, doi:10.1016/j.cell.2015.08.011 (2015). [PubMed: 26321680]

35. Liu N et al. N(6)-methyladenosine-dependent RNA structural switches regulate RNA-protein interactions. Nature 518, 560–564, doi:10.1038/nature14234 (2015). [PubMed: 25719671]
36. Shi H, Wei J & He C Where, When, and How: Context-Dependent Functions of RNA Methylation Writers, Readers, and Erasers. Molecular cell 74, 640–650, doi:10.1016/j.molcel.2019.04.025 (2019). [PubMed: 31100245]
37. Yang Y, Hsu PJ, Chen YS & Yang YG Dynamic transcriptomic m(6)A decoration: writers, erasers, readers and functions in RNA metabolism. Cell Res 28, 616–624, doi:10.1038/s41422-018-0040-8 (2018). [PubMed: 29789545]
38. Meyer KD & Jaffrey SR Rethinking m(6)A Readers, Writers, and Erasers. Annu Rev Cell Dev Biol 33, 319–342, doi:10.1146/annurev-cellbio-100616-060758 (2017). [PubMed: 28759256]
39. Liu X-M, Zhou J, Mao Y, Ji Q & Qian S-B Programmable RNA N6-methyladenosine editing by CRISPR-Cas9 conjugates. Nature Chemical Biology, doi:10.1038/s41589-019-0327-1 (2019).
40. Abudayyeh OO et al. RNA targeting with CRISPR-Cas13. Nature 550, 280–284, doi:10.1038/nature24049 (2017). [PubMed: 28976959]
41. East-Seletsky A et al. Two distinct RNase activities of CRISPR-C2c2 enable guide-RNA processing and RNA detection. Nature 538, 270–273, doi:10.1038/nature19802 (2016). [PubMed: 27669025]
42. Abudayyeh OO et al. C2c2 is a single-component programmable RNA-guided RNA-targeting CRISPR effector. Science 353, aaf5573, doi:10.1126/science.aaf5573 (2016). [PubMed: 27256883]
43. Li F et al. A Radioactivity-Based Assay for Screening Human m6A-RNA Methyltransferase, METTL3-METTL14 Complex, and Demethylase ALKBH5. Journal of biomolecular screening 21, 290–297, doi:10.1177/1087057115623264 (2016). [PubMed: 26701100]
44. Cox DBT et al. RNA editing with CRISPR-Cas13. Science, doi:10.1126/science.aaq0180 (2017).
45. Abudayyeh OO et al. A cytosine deaminase for programmable single-base RNA editing. Science 365, 382, doi:10.1126/science.aax7063 (2019). [PubMed: 31296651]
46. Slaymaker IM et al. High-Resolution Structure of Cas13b and Biochemical Characterization of RNA Targeting and Cleavage. Cell Reports 26, 3741–3751.e3745, doi:10.1016/j.celrep.2019.02.094 (2019). [PubMed: 30917325]
47. Schellenberger V et al. A recombinant polypeptide extends the in vivo half-life of peptides and proteins in a tunable manner. Nat Biotechnol 27, 1186–1190, doi:10.1038/nbt.1588 (2009). [PubMed: 19915550]
48. Meyer KD et al. Comprehensive analysis of mRNA methylation reveals enrichment in 3' UTRs and near stop codons. Cell 149, 1635–1646, doi:10.1016/j.cell.2012.05.003 (2012). [PubMed: 22608085]
49. Nelles DA et al. Programmable RNA Tracking in Live Cells with CRISPR/Cas9. Cell 165, 488–496, doi:10.1016/j.cell.2016.02.054 (2016). [PubMed: 26997482]
50. Liu N et al. Probing N6-methyladenosine RNA modification status at single nucleotide resolution in mRNA and long noncoding RNA. RNA 19, 1848–1856, doi:10.1261/rna.041178.113 (2013). [PubMed: 24141618]
51. Cui Q et al. m(6)A RNA Methylation Regulates the Self-Renewal and Tumorigenesis of Glioblastoma Stem Cells. Cell Rep 18, 2622–2634, doi:10.1016/j.celrep.2017.02.059 (2017). [PubMed: 28297667]
52. Zhang S et al. m(6)A Demethylase ALKBH5 Maintains Tumorigenicity of Glioblastoma Stem-like Cells by Sustaining FOXM1 Expression and Cell Proliferation Program. Cancer Cell 31, 591–606 e596, doi:10.1016/j.ccell.2017.02.013 (2017). [PubMed: 28344040]
53. Geula S et al. m6A mRNA methylation facilitates resolution of naive pluripotency toward differentiation. Science 347, 1002–1006, doi:10.1126/science.1261417 (2015). [PubMed: 25569111]
54. Garcia-Campos MA et al. Deciphering the "m(6)A Code" via Antibody-Independent Quantitative Profiling. Cell 178, 731–747.e716, doi:10.1016/j.cell.2019.06.013 (2019). [PubMed: 31257032]
55. Zhang Z et al. Single-base mapping of m6A by an antibody-independent method. Science Advances 5, eaax0250, doi:10.1126/sciadv.aax0250 (2019). [PubMed: 31281898]

56. Imanishi M, Tsuji S, Suda A & Futaki S Detection of N6-methyladenosine based on the methyl-sensitivity of MazF RNA endonuclease. Chemical Communications 53, 12930–12933, doi:10.1039/C7CC07699A (2017). [PubMed: 29154383]

57. Bartosovic M et al. N6-methyladenosine demethylase FTO targets pre-mRNAs and regulates alternative splicing and 3′-end processing. Nucleic Acids Research 45, 11356–11370, doi:10.1093/nar/gkx778 (2017). [PubMed: 28977517]

58. Xiao W et al. Nuclear m6A Reader YTHDC1 Regulates mRNA Splicing. Molecular Cell 61, 507–519, doi:10.1016/j.molcel.2016.01.012 (2016). [PubMed: 26876937]

59. O'Connell MR et al. Programmable RNA recognition and cleavage by CRISPR/Cas9. Nature 516, 263–266, doi:10.1038/nature13769 (2014). [PubMed: 25274302]

60. Alarcón CR, Lee H, Goodarzi H, Halberg N & Tavazoie SF N6-methyladenosine marks primary microRNAs for processing. Nature 519, 482, doi:10.1038/nature14281 (2015). [PubMed: 25799998]

Methods References

61. Gaudelli NM et al. Programmable base editing of A*T to G*C in genomic DNA without DNA cleavage. Nature 551, 464–471, doi:10.1038/nature24644 (2017). [PubMed: 29160308]

62. Dominissini D, Moshitch-Moshkovitz S, Salmon-Divon M, Amariglio N & Rechavi G Transcriptome-wide mapping of N(6)-methyladenosine by m(6)A-seq based on immunocapturing and massively parallel sequencing. Nat Protoc 8, 176–189, doi:10.1038/nprot.2012.148 (2013). [PubMed: 23288318]

63. Livak KJ & Schmittgen TD Analysis of relative gene expression data using real-time quantitative PCR and the 2(-Delta Delta C(T)) Method. Methods 25, 402–408, doi:10.1006/meth.2001.1262 (2001). [PubMed: 11846609]

64. Cui X et al. MeTDiff: a novel differential RNA methylation analysis for MeRIP-Seq data. IEEE/ACM transactions on computational biology and bioinformatics 15, 526–534 (2015).

65. Heinz S et al. Simple combinations of lineage-determining transcription factors prime cis-regulatory elements required for macrophage and B cell identities. Molecular cell 38, 576–589, doi:10.1016/j.molcel.2010.05.004 (2010). [PubMed: 20513432]

66. Law CW, Chen Y, Shi W & Smyth GK voom: precision weights unlock linear model analysis tools for RNA-seq read counts. Genome biology 15, R29, doi:10.1186/gb-2014-15-2-r29 (2014). [PubMed: 24485249]

67. Ritchie ME et al. limma powers differential expression analyses for RNA-sequencing and microarray studies. Nucleic Acids Research 43, e47–e47, doi:10.1093/nar/gkv007 (2015). [PubMed: 25605792]

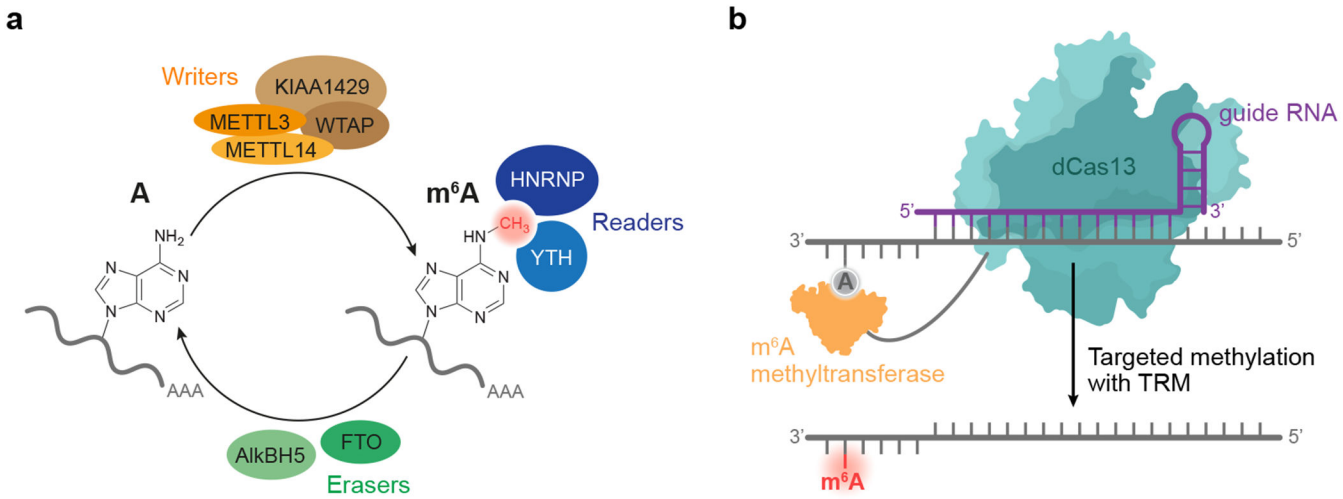

Figure 1. Overview of cellular modification of adenine to m^{6}A in mRNA, and design of a targeted RNA methylation system.

(a) METTL3 and METTL14 form a "writer" complex that catalyzes *S*-adenosyl methionine (SAM)-dependent methylation of the N^6 of adenine in cellular mRNA. Additional components influence the formation and activity of this core complex. FTO and ALKBH5 ("erasers") remove the methyl group of m^{6}A. "Readers" recognize the mark on RNA and direct it to various outcomes. **(b)** Proposed strategy for targeted RNA methylation (TRM). A programmable RNA-binding protein such as dCas13 when fused to an appropriate methyltransferase complex mediates the guide RNA-specified methylation of A to m^{6}A site-specifically in a target transcript.

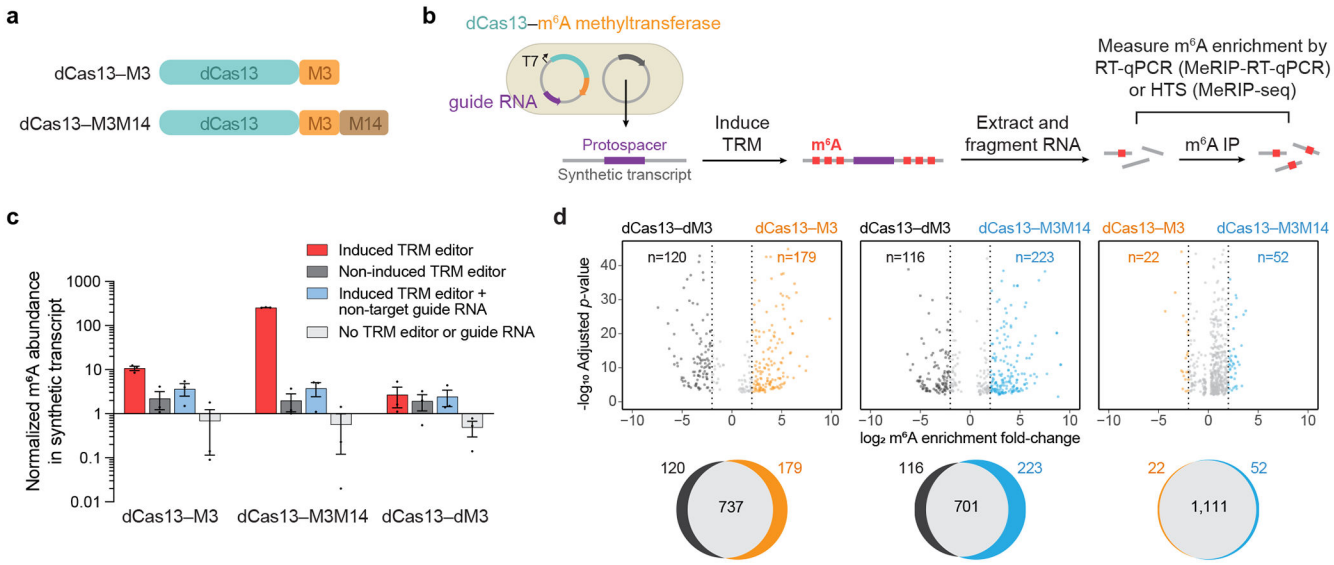

Figure 2. Validation of targeted RNA methylation (TRM) in *E. coli*.

(a) METTL3$^{273\text{-}580}$ (M3) or METTL3$^{359\text{-}580}$–(GGS)$_{10}$–METTL14$^{111\text{-}456}$ (M3M14) methyltransferases were fused to catalytically-impaired PspCas13b Δ984-1090 (dCas13) to generate dCas13–M3 or dCas13–M3M14 TRM editors. **(b)** Plasmids transformed into *E. coli* encode IPTG-inducible TRM editors with a guide RNA targeting a synthetic transcript. After targeted methylation, cellular total RNA was purified, fragmented, and immunoprecipitated with anti-m^{6}A antibodies. Enrichment of m^{6}A was measured by target-specific RT-qPCR (MeRIP-RT-qPCR) or transcriptome-wide high-throughput sequencing (MeRIP-seq). **(c)** Target transcript m^{6}A abundance measured by MeRIP-RT-qPCR under four conditions: induced TRM editor with transcript-targeting guide, non-induced editor with transcript-targeting guide, induced editor with a non-target guide, and cells lacking TRM editor and guide plasmid. The methyltransferase-inactive control was dCas13–M3^{D395A} (dCas13–dM3). Values and error bars reflect the mean±s.e.m. of n=3 independent biological replicates. **(d)** Top: differential m^{6}A enrichment of all methylated adenines in *E. coli* expressing synthetic transcript-targeting guide RNAs and the indicated TRM editors. For the comparisons above, only differentially methylated sites with statistical significance (P<0.001) are shown. Bottom: Venn diagrams depicting overlap of all methylated m^{6}A sites for the above comparisons. 42,418 total m^{6}A motifs (RRACH) are susceptible to modification within the *E. coli* transcriptome. MeRIP-seq analysis was performed with n=3 independent biological replicates. Statistical significance was calculated using a logs likelihood-ratio test with false discovery rate correction.

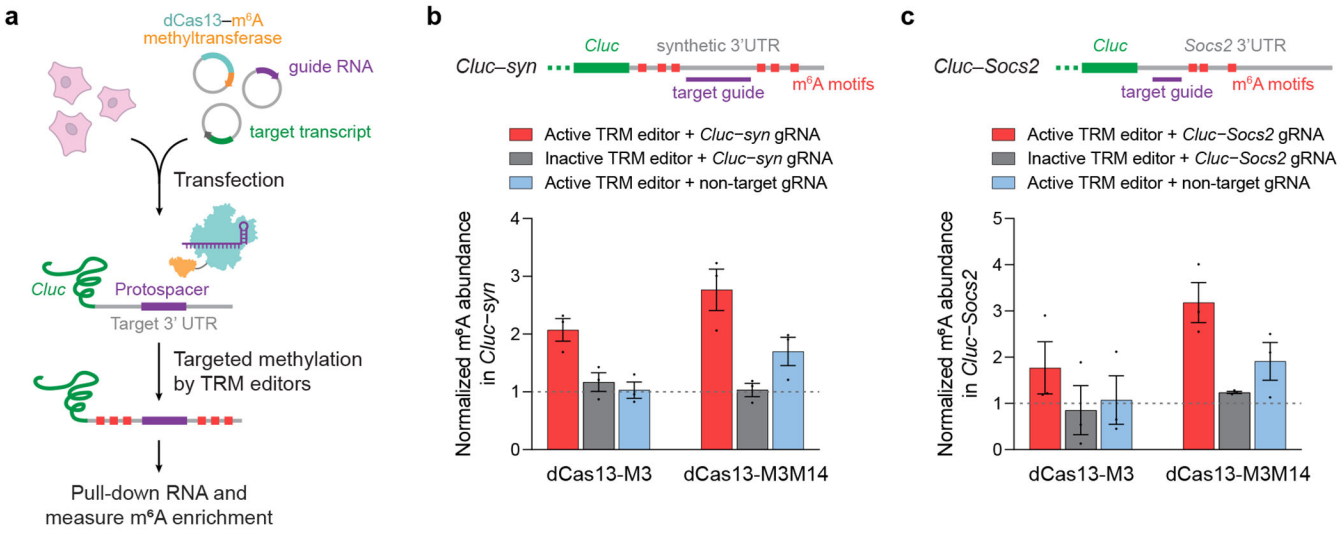

Figure 3. Methylation of reporter transcripts in human cells.

(a) HEK293T cells were transfected with plasmids encoding a TRM editor, Cas13 guide RNA, and the targeted *Cluc* reporter transcript containing a 3' UTR methylation target. **(b)** Methylation of a synthetic 3' UTR fused to *Cypridina* luciferase (*Cluc–syn*) by TRM editors. **(c)** Methylation of the *Socs2* 3' UTR fused to *Cypridina* luciferase (*Cluc–Socs2*) by TRM editors. Inactive TRM editors contain a methyltransferase-inactivating D395A mutation within M3. Values and error bars reflect the mean±s.e.m. of n=3 independent biological replicates.

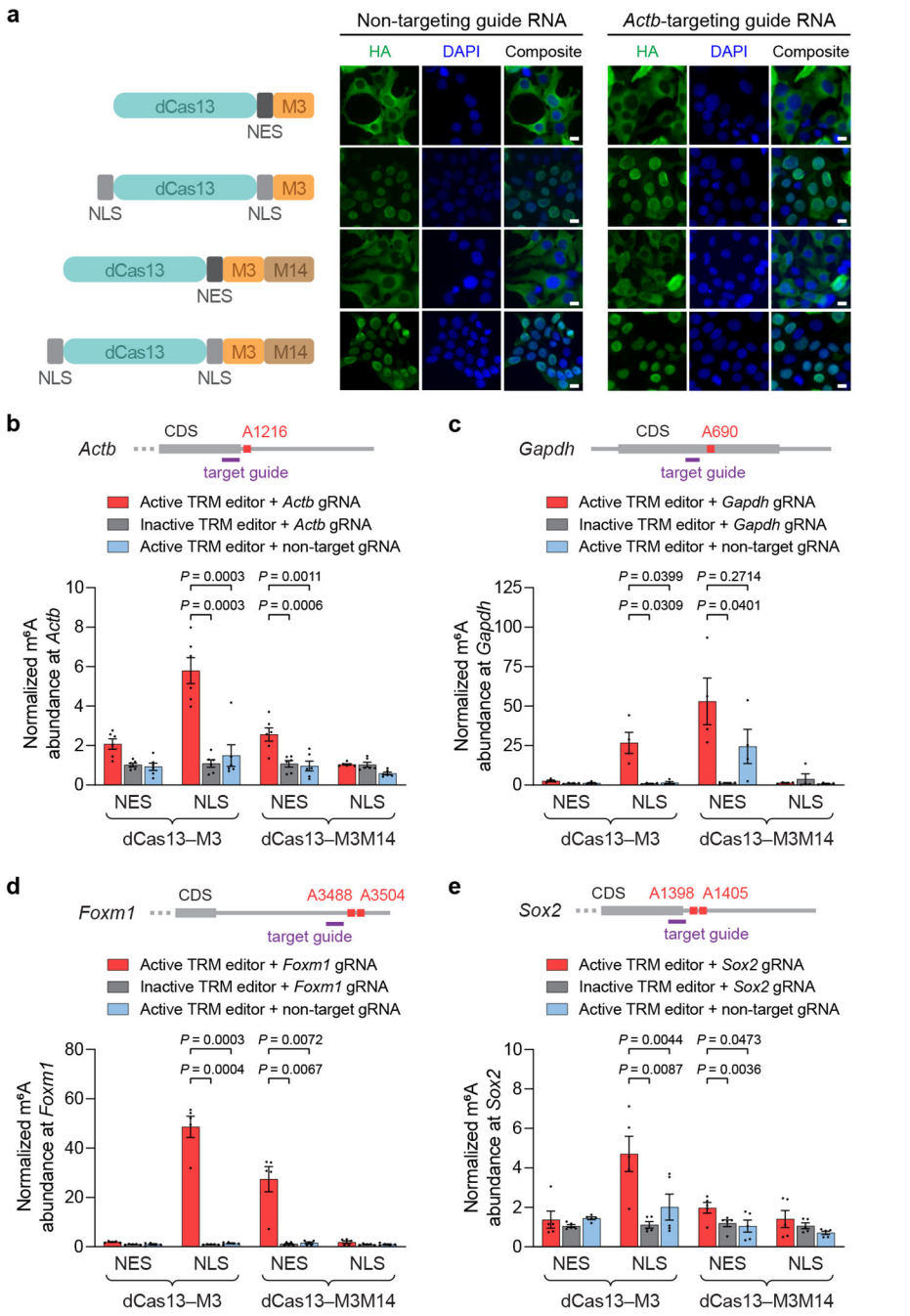

Figure 4. Cellular localization of TRM editors and targeted methylation of endogenous transcripts in human cells.

(a) Left: nucleus- and cytoplasm-localized TRM editor variants. NES = nuclear export signal; NLS = nuclear localization signal. Right: representative immunofluorescence images of HEK293T cells transfected with HA-tagged TRM editors and non-targeting or *Actb*-targeting guide RNAs. Green = HA tag; blue = DAPI. Scale bars represent 10 μm. The experiment was independently performed twice with similar results. **(b-e)** Methylation by nucleus- and cytoplasm-localized TRM editors targeting endogenous (b) *Actb* A1216, (c)

Gapdh A690, (d) *Foxm1* A3488 and A3504, and (e) *Sox2* A1398 and A1405. Guide RNAs used for targeting each transcript are shown in purple. Inactive TRM editors contain a methyltransferase-inactivating D395A mutation within M3. Values and error bars reflect the mean±s.e.m. of n=6 **(b)**, n=4 **(c)**, or n=5 **(d,e)** independent biological replicates. *P* values were calculated using a two-tailed Student's *t*-test.

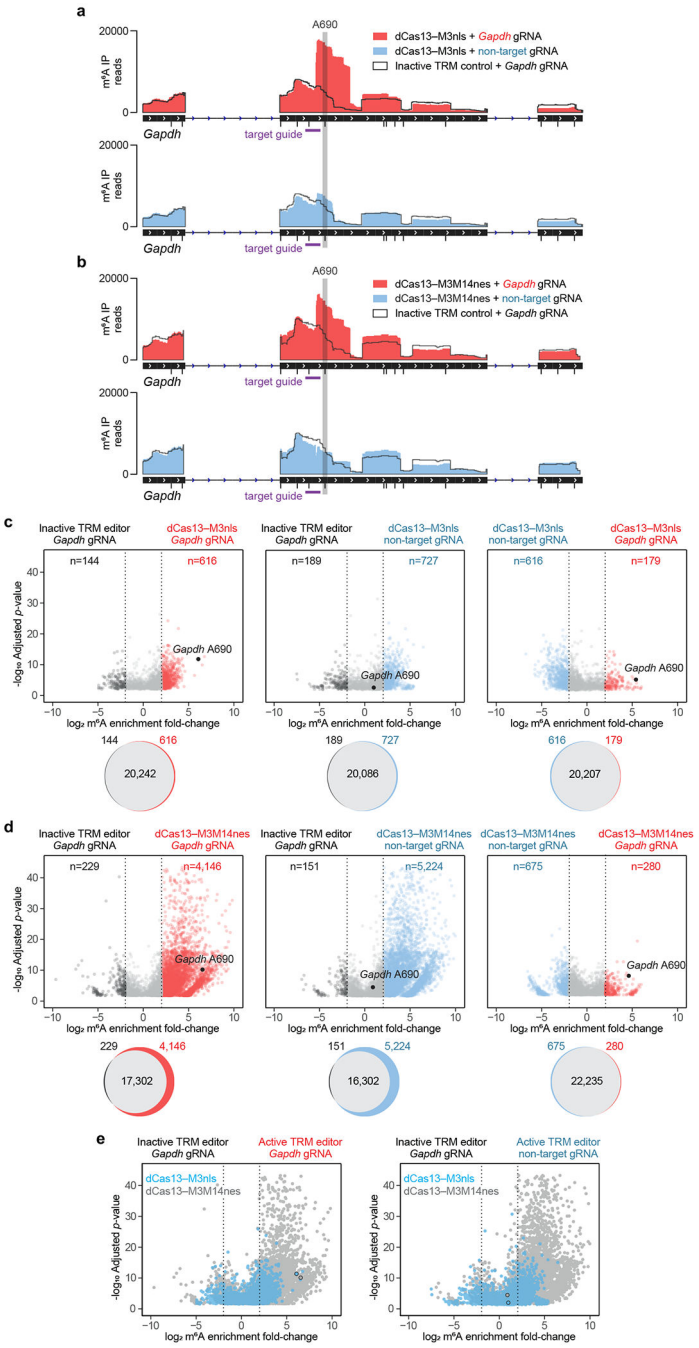

Figure 5. Specificity and off-target methylation of TRM editors.

(a,b) *Gapdh* read coverage of m^{6}A-immunoprecipitated (m^{6}A IP) RNA from MeRIP-seq of transfected HEK293T cells. *Gapdh* A690 was targeted with (a) dCas13–M3nls or (b) dCas13–M3M14nes with the following conditions: active editor with a target guide RNA, inactive editor with a target guide RNA, and active editor with a non-target guide RNA. All DRACH motifs susceptible to TRM modification are shown as black tick marks underneath the IGV track. The target guide RNA (purple) and targeted A690 site (grey) are shown. **(c,d)** Differential m^{6}A enrichment of >21,000 methylated sites in HEK293T cells transfected with

(c) dCas13–M3nls or (d) dCas13–M3M14nes and *Gapdh* A690-targeting or non-target guide RNAs. Top: differential methylation of m^6A sites between conditions indicated above. Only differentially methylated sites with statistical significance ($P<0.001$) are shown. Bottom: Venn diagrams depicting overlap of all methylated m^6A sites for the above comparisons. **(e)** Overlay of dCas13–M3nls (blue) and dCas13–M3M14nes (grey) differential methylation with the following comparisons: left, active editors with *Gapdh* guide RNAs vs. inactive editors with *Gapdh* guide RNAs; right, active editors with non-target guide RNAs vs. inactive editors with *Gapdh* guide RNAs. The targeted *Gapdh* A690 site is outlined in black. Inactive TRM editors contain a methyltransferase-inactivating D395A mutation within M3. MeRIP-seq analysis was performed with n=5 independent biological replicates. Statistical significance was calculated using a logs likelihood-ratio test with false discovery rate correction.

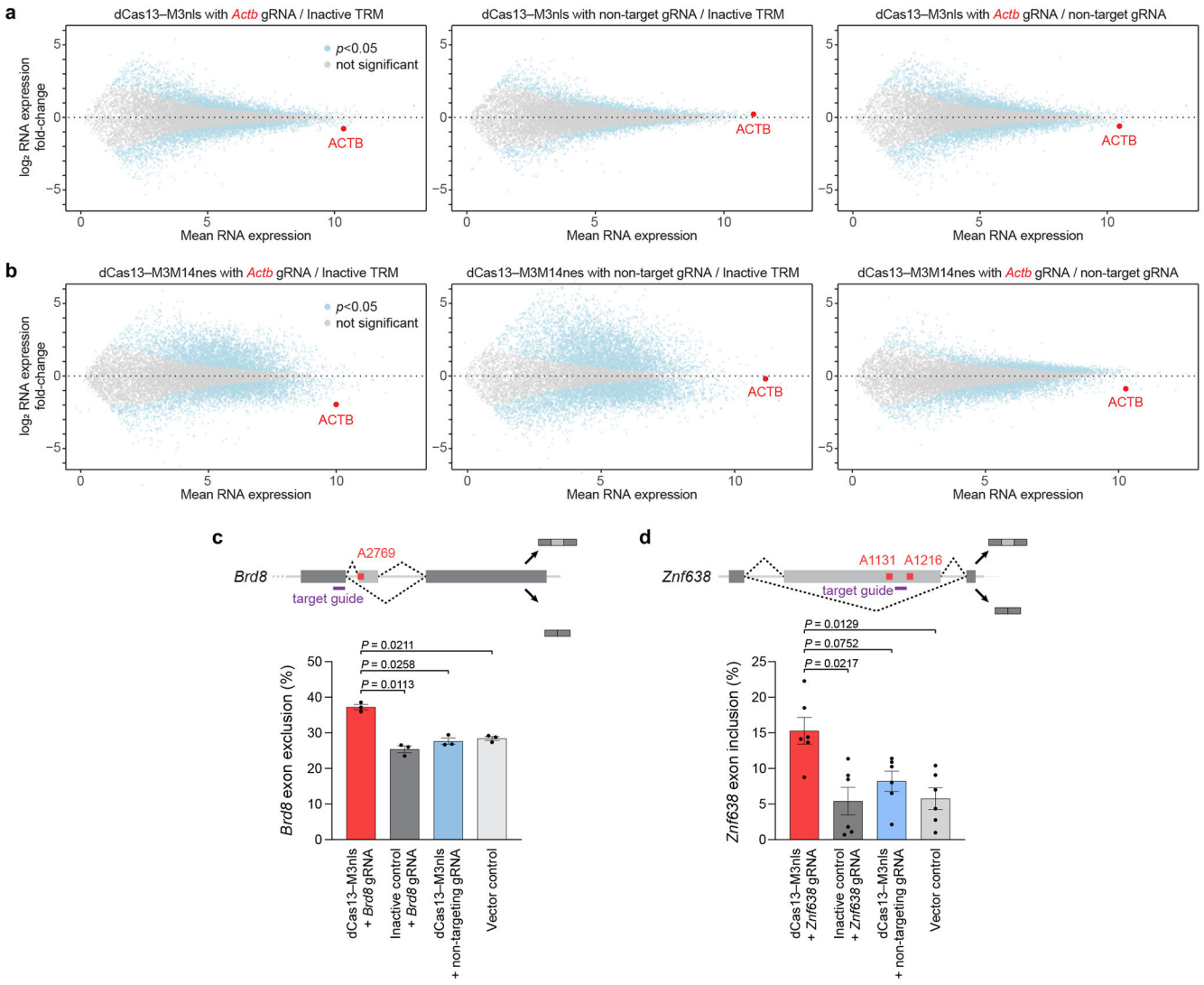

Figure 6. TRM effect on RNA abundance and alternative splicing.

Differential RNA expression of HEK293T cells transfected with **(a)** dCas13–M3nls or **(b)** dCas13–M3M14nes and either *Actb* A1216-targeting or non-targeting guide RNAs. The targeted *Actb* gene is marked in red. Inactive TRM control indicates editors containing a methyltransferase-inactivating M3 D395A mutation with an *Actb*-targeting guide RNA. Non-target gRNA indicates methyltransferase-active TRM editors with a non-targeting guide RNA as a control. Differential RNA-seq analysis was performed with n=5 independent biological replicates. Statistical significance was calculated using a two-tailed Student's *t*-test with false discovery rate correction. Alternative splicing of **(c)** *Brd8* and **(d)** *Znf638* in HEK293T cells transfected with dCas13–M3nls and the indicated guide RNAs (purple) for targeting m^{6}A sites shown (red). Exon exclusion or inclusion indicates the percentage of RNA isoform lacking or containing the alternatively-spliced exon, respectively. Values and error bars reflect the mean±s.e.m. of n=3 **(c)** or n=6 **(d)** independent biological replicates. *P* values were calculated using a two-tailed Student's *t*-test.